

## The stability of Ca–Na pyroxene in low-grade metabasites of high-pressure intermediate facies series

SHIGENORI MARUYAMA<sup>1</sup> AND J. G. LIOU

Department of Geology  
Stanford University, Stanford, California 94305

### Abstract

Minor metamorphic Ca–Na pyroxene occurs as minute crystals and as thin rims around primary augites in metabasites intermediate between the prehnite–pumpellyite (PP) and pumpellyite–actinolite (PA) facies in the Sanbagawa belt, Shikoku, Japan. Their compositions vary systematically with mineral paragenesis, from augite to acmite, with a constant jadeite component of about 20 mol%. The Ca–Na pyroxenes in the pumpellyite-bearing assemblages contain a very low acmite component ( $Ac_0Aug_{80}Jd_{20}$ ), which increases through  $Ac_{25}Aug_{55}Jd_{20}$  in the alkali amphibole-bearing and  $Ac_{60}Aug_{25}Jd_{15}$  in the hematite-bearing assemblages, finally attaining an aegirine composition ( $Ac_{65}Aug_{10}Jd_{25}$ ) in the magnetite-bearing assemblages. They are distinguished from relict igneous augites chemically by very low OPX and  $TiO_2$  contents, and morphologically by fibrous crystal habit.

The pyroxene-bearing metabasites contain assemblages of chlorite + pyroxene + pumpellyite (+ epidote, actinolite, alkali amphibole, stilpnomelane, hematite and magnetite), which are incompatible with the higher grade and widely developed pumpellyite–actinolite facies assemblage, epidote + chlorite ( $X_{Fe} = 0.50$ ) + actinolite + pumpellyite. The reaction: augite + chlorite = pumpellyite + actinolite +  $H_2O$  has been suggested for such a transition. The stability relations of augite + chlorite + pumpellyite were analyzed from comparative mineral parageneses in low-grade metabasites from New Caledonia, New Zealand, and the Appalachians. The assemblage may have a wedge-shaped P–T space bounded against the high-*T* pumpellyite–actinolite facies by the above reaction and against the low-*T* prehnite–pumpellyite facies by the reaction prehnite + actinolite = augite + chlorite with probable negative slope. From the mineral parageneses in the metabasites of the Sanbagawa belt and elsewhere, it is concluded that the Ca–Na pyroxenes occur within a restricted P–T space between the prehnite–pumpellyite and pumpellyite–actinolite facies.

### Introduction

Clinopyroxenes are common in high-grade metamorphic rocks such as amphibolite, granulite and eclogite and also appear in blueschist facies metabasites. The characteristic clinopyroxenes in amphibolite and granulite are augitic to diopsidic in composition whereas those in eclogite and blueschists contain jadeite or jadeite-rich omphacite (e.g., Deer et al., 1978). Recently, sodic salite has been described in meta-syenites of the albite–epidote amphibolite facies (Droop, 1982). Diopsidic pyroxenes are common in some deep geothermal drill hole samples (e.g., Cerro Prieto by Bird et al., 1984 and Schiffman et al., 1984, and Larderello by Cavarretta et al., 1982). In spite of these occurrences, clinopyroxenes are typically absent in rocks of low or medium metamorphic grade. If they occur in metabasalts of zeolite, prehnite–pumpel-

lyite or even greenschist facies, they are generally regarded as relict igneous augites (e.g., Coleman, 1977).

This paper describes some unusual occurrences of Ca–Na clinopyroxene metabasites from the lower zone of the pumpellyite–actinolite facies from a small area of the Sanbagawa belt, Japan. Relict primary igneous augites also occur in these metabasites. Evidence from textures, chemical characteristics, and phase equilibria described in this paper indicates that the Ca–Na clinopyroxenes were formed during the Sanbagawa metamorphism at conditions between the prehnite–pumpellyite and pumpellyite–actinolite facies.

### Field relations

The Ca–Na pyroxene-bearing metabasites occur in a small area in Kochi, central Shikoku, Japan (Fig. 1). Regional geology, metamorphic zones, and mineral parageneses and chemistries in adjacent areas have been described by Banno (1964), Nakajima et al. (1977), and Aiba (1982).

<sup>1</sup>Present address: Department of Earth Sciences, Toyama University, Toyama 930, Japan.

The Sanbagawa–Chichibu terrain is composed mainly of pelitic-psammitic and mafic schists with subordinate amounts of quartzitic and calcareous rocks. Fossil ages range from Late Carboniferous to Early Jurassic (Kanmera, 1969; Matsuda, 1978, Isozaki et al., 1981); radiometric ages for metamorphism range from 110 to 67 m.y. (Ueda et al., 1977).

Banno (1964) concluded that the Sanbagawa metamorphism has affected the northern half of the Chichibu belt; the metamorphic grade decreases gradually from the epidote amphibolite facies in the north to the blueschist facies in the south. In between, 4 metamorphic zones from high to low grades have been delineated: biotite zone and garnet zone (both based on metapelite assemblages); pumpellyite-absent zone and pumpellyite zone (both based on metabasite assemblages). A wide-spread occurrence of the prehnite–pumpellyite zone to the south of the boundary between the Sanbagawa and the Chichibu metamorphic terrain has been recognized by Hashimoto et al. (1970). As shown in Figure 1, E–W metamorphic zones of the greenschist, pumpellyite–actinolite and prehnite–pumpellyite facies and the Kurosegawa tectonic zone are subparallel. The study area is located within the pumpellyite–actinolite zone about 2 km north of the boundary between the pumpellyite–actinolite and prehnite–pumpellyite zones.

The Mikabu Carboniferous ophiolite complex occurs within the study area between the Sanbagawa and the Chichibu belts. It is 4 x 50 km in dimensions and consists predominantly of mafic lavas and breccias (hyaloclastites) with subordinate amounts of ultramafic, gabbro, diabase and radiolarian chert (Fig. 1). The ophiolite complex is bounded to the north by a fault and is conformable with the overlying clastic rocks of the Chichibu belt to the south. However, metamorphism took place after its emplacement, and the metamorphic grade is continuous across the fault. The study area, therefore, contains a small section of Sanbagawa metamorphic zones. We focus our study on paragenesis and chemistry of minerals from the metabasites of the ophiolite complex, with emphasis on the paragenesis and stability relations of clinopyroxene-bearing assemblages. Mineral parageneses of the prehnite–pumpellyite, augite–chlorite and pumpellyite–actinolite zones are shown in Figure 2.

### Petrography of metabasites

Original structures (pillows, hyaloclastites, and feeder dikes) and textures (ophitic, subophitic, intersertal and intergranular) are well preserved in the metamafics from the studied area. Primary plagioclase is completely altered to albite associated with pumpellyite±phengite±epidote. Some chlorite pseudomorphs after olivine are recognized by characteristic olivine crystal forms with tiny inclusions of spinel (mostly altered to magnetite). Relict diopside–augites are common and are replaced partially by metamorphic Ca–Na pyroxene, actinolite, or sodic amphibole along cleavages and irregular cracks.

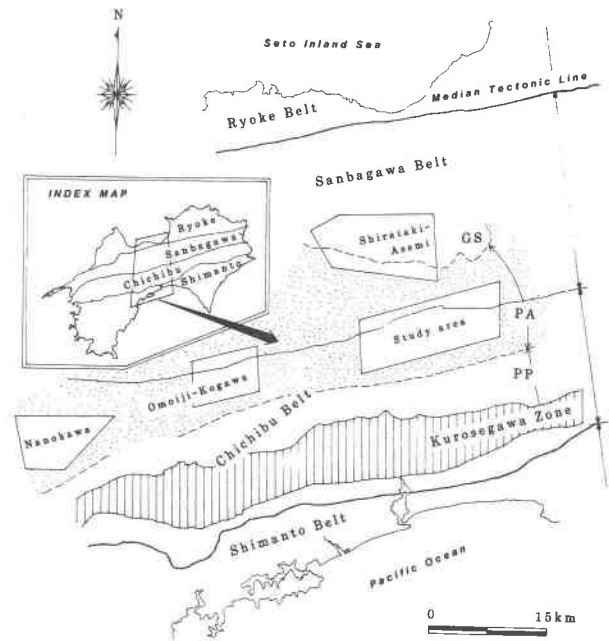


Fig. 1. Location of the study area and distribution of greenschist (GS), pumpellyite–actinolite (PA) and prehnite–pumpellyite (PP) facies rocks in central Shikoku, Japan (Hashimoto et al., 1970; Banno et al., 1978). The Mikabu ophiolite complex is located within the study area.

Igneous oxides are completely recrystallized to sphene and have preserved their crystal forms.

Mineral assemblages from 250 thin sections were identified. The assemblages can be divided into three groups based on the occurrence of calcite and metamorphic pyroxene: (1) calcite-free and pyroxene-free [210], (2) calcite-free and pyroxene-bearing [35], and (3) calcite-bearing and pyroxene-free [5]. The numbers in brackets

Schematic Mineral Parageneses for metabasites in Central Shikoku, Japan

Mineral	Zone	Prehnite - Pumpellyite	Augite - Chlorite	Pumpellyite - Actinolite
prehnite		—————		
pumpellyite		—————		
actinolite			—————	
Na-amphibole			.....	.....
clinopyroxene			.....	.....
epidote		.....		
albite		—————		
chlorite			—————	
References		Hashimoto et al. (1970)	this study	this study & Nakajima et al. (1977)

Fig. 2. Schematic mineral parageneses for metabasites of the prehnite–pumpellyite, augite–chlorite and pumpellyite–actinolite zones in central Shikoku, Japan. Stilpnomelane, hematite, magnetite, sphene and muscovite may occur as accessory phases.

Table 1. Mineral assemblages of metabasites\*

A. Carbonate- and pyroxene-free assemblages	
Epidote-chlorite-actinolite-pumpellyite	
Chlorite-pumpellyite-riebeckite+stilpnomelane	
Epidote-chlorite-pumpellyite+stilpnomelane	
B. Carbonate-free and pyroxene-bearing assemblages (+clinopyroxene, +chlorite)	
Epidote-actinolite+pumpellyite	
Epidote-riebeckite+stilpnomelane	
Epidote-pumpellyite+riebeckite	
Epidote-riebeckite+stilpnomelane+magnetite	
Epidote-actinolite-pumpellyite+hematite	
C. Carbonate-bearing and pyroxene-free assemblages (+calcite)	
Stilpnomelane	
Chlorite-riebeckite+epidote	
Pumpellyite-riebeckite	
Epidote-chlorite-pumpellyite	
* All assemblages include albite, quartz and sphene (+ phengite and apatite).	

refer to the total number of thin sections investigated from each group. Observed assemblages are listed in Table 1 and include minerals observed within a single thin section, although Zen (1974) restricted stable assemblages to those within a domain less than 1 mm wide. The size of equilibrated domains for Sanbagawa metamorphic rocks has been discussed by Nakajima et al. (1977). They concluded that equilibrium is almost reached for minerals within a thin section, except for vein minerals of a later stage or actinolite needles within albite prisms. For the present study we adopt the conclusion of Nakajima et al. (1977).

Minor phases include stilpnomelane, hematite, magnetite, pyrite and chalcopyrite. Carbonate was determined to be calcite rather than aragonite by testing with Feigl's solution. Sphene and phengitic mica are ubiquitous. Characteristic features of each group are described below:

Most metabasites (210 samples) from the study area contain neither calcite or pyroxene.<sup>2</sup> Mineral assemblages of this group are further subdivided into two subgroups; the first is characterized by epidote-chlorite-actinolite-pumpellyite, and the second by pumpellyite-riebeckite. Stilpnomelane appears only in the second subgroup. All analyzed chlorite have Fe/(Fe + Mg) ratio smaller than 0.68; the chlorites in the first subgroup are lower in Fe than those in the second subgroup.

Most of the calcite-free and pyroxene-bearing metabasites contain fewer than five coexisting phases, although two sections contain 6 phases. The characteristic feature of the assemblages is the stable association of pyroxene + chlorite. Among calcite-bearing metabasites, stilpnome-

lane-calcite and chlorite-calcite assemblages have significance for our later discussion of  $X_{\text{Co}_2}$  the fluid phase.

### Mineral chemistry

Compositions of minerals were analyzed using a Hitachi microprobe at Kanazawa University, Japan. Representative analyses are listed in Table 2. Complete analyses of minerals are available from the senior author.

### Pyroxene

Metamorphic pyroxene occurs as an epitaxial fringe around and metasomatically replacing the igneous augites, and rarely as discrete fibrous crystals in the vein or matrix. Some pyroxene occurrences are shown in Figure 3. In most rocks, the relict augites are nearly colorless to pale brown, whereas the metamorphic aegirine-augite and aegirine ubiquitously show light green to pale green colors. Some metamorphic augites are the same color as igneous augites but can be differentiated by distinct differences in chemical composition and crystal morphology. The igneous pyroxenes are characterized by low Ca and high Ti- and Cr-contents and the metamorphic pyroxenes commonly have anhedral fibrous crystal forms. The  $\text{Fe}_2\text{O}_3$  contents of pyroxenes were calculated on the basis of a total of 4 cations for 6 oxygens. End-members were computed following the method of Banno (1959).

Figure 4 is a plot of analyses of both igneous and metamorphic pyroxenes in terms of  $\text{TiO}_2$  content and major pyroxene components En-Fs-Di-Hd. All metamorphic pyroxenes contain less than 0.03 Ti atoms per formula unit and less than 0.01 wt.%  $\text{Cr}_2\text{O}_3$ , whereas igneous pyroxenes either are chromian diopside with  $\text{Cr}_2\text{O}_3$  up to 1.07 wt.% or have greater than 0.02 Ti atoms per formula unit. Igneous pyroxenes have much more restricted augite compositions in pyroxene quadrilateral plots than the metamorphic pyroxenes, which are characteristically higher in Fe and lower in Mg contents and are highly variable in composition depending on mineral assemblages. The results of end-member calculations indicate that more than 98% of the components of the metamorphic pyroxenes can be expressed by the Aug (Di + Hd)-Jd-Ac system in Figure 5. Three features are apparent in Figure 5: (1) Although considerable compositional scattering due to chemical zoning is shown in Figures 4 and 5, pyroxene compositions vary systematically according to assemblages. Such variation suggests that chemical equilibrium may have been nearly attained during metamorphism. However, pyroxenes of the high-variance assemblage epidote-chlorite-pyroxene contain 0 to 30 mol% acmite component. The pyroxenes coexisting with epidote-chlorite-pumpellyite-actinolite are restricted in composition to close to the augite-jadeite join. The crossite- and riebeckite-bearing metabasites contain pyroxenes intermediate in composition between augite and acmite. Pyroxenes coexisting with hematite or magnetite are most acmite-rich. (2) The maximum jadeite content of

<sup>2</sup>Unless specified, pyroxenes described in this paper are of metamorphic origin.

most pyroxenes, regardless of mineral assemblage, is about 20 mol %. (3) Chemical zoning of most clinopyroxene crystals is of a progressive type, i.e., the pyroxene rims are enriched in jadeite component compared to the cores. Some zoned pyroxene grains may contain less jadeite rim; such features will be described later.

### *Epidote*

Epidote is a common phase in these metabasites. Analyzed epidotes vary in pistacite component from 18 to 36 mol%, with a maximum frequency at 33–34%, as shown in Figure 6. Maximum pistacite contents (35–36%) occur in epidotes which coexist with hematite; epidotes in magnetite-bearing rocks have pistacite contents of 18–27%. Such epidote compositions are consistent with those from lower pumpellyite–actinolite facies rocks elsewhere in the Sanbagawa belt (e.g., Nakajima, 1982).

### *Actinolite*

Actinolite occurs as fibrous aggregates around relict augite and crossite-riebeckite, or as independent prismatic needles in the fine-grained metabasite matrix. Some actinolites are close to the ideal formula,  $\text{Ca}_2(\text{Mg}, \text{Fe})_5\text{Si}_8\text{O}_{22}(\text{OH})_2$ . Actinolites coexisting with alkali-amphibole, however, may contain up to 37% alkali-amphibole end-member. We estimate the  $\text{Fe}_2\text{O}_3$  content of the amphiboles by assuming zero A-site occupancy. This assumption is justified for the metamorphic grade of lower pumpellyite–actinolite facies, by the extremely low pargasite contents in amphiboles from quartz-bearing rocks, and by the calculated Si content of 7.48–8.02 for the analyzed Ca-amphiboles. The compositions are plotted in a ternary diagram in terms of actinolite, glaucophane and riebeckite end-members in Figure 7; the results support the existence of the compositional gap that was documented by Coleman and Papike (1968) and Toriumi (1975). Intermediate amphiboles between riebeckite and actinolite with  $X_{\text{Mg}} = 0.71$  occur in some metamafics from the adjacent Omoiji-Kogawa area (Nakajima et al., 1977) and are shown by the closed circles in Figure 7. Relations such as those shown in Figure 7 suggest that the metamorphic grade of the clinopyroxene-bearing metabasites from the study area is slightly lower than that of the Omoiji-Kogawa area.

### *Crossite-riebeckite*

This amphibole also occurs as fine-grained prismatic crystals around relict augite. It shows distinct pleochroism from blue to violet and contains between 7 and 50 mol % of the glaucophane endmember. Some sodic amphiboles entirely rimmed by actinolite contain up to 35% actinolite endmember (Fig. 7).

### *Pumpellyite*

Pumpellyite occurs in amygdules, replacing plagioclase in veins with albite and/or quartz, and as fine-grained

aggregates in the matrix of metabasites. Compositions of pumpellyites are plotted in Figure 8 in terms of  $2\text{Al}-\text{Fe}^*-\text{Mg}$  of Coombs et al. (1976) together with those of chlorite and stilpnomelane. Pumpellyite compositions vary in terms of  $\text{Al} \rightleftharpoons \text{Fe}^{3+}$  substitution; Mg contents also are not constant, suggesting minor  $\text{Mg} \rightleftharpoons \text{Fe}^{2+}$  substitution. The pumpellyite coexisting with stilpnomelane as shown in Figure 8 contains higher  $\text{Fe}^{3+}$  than other analyzed pumpellyites from the study area.

### *Chlorite*

Chlorite is ubiquitous in these metabasites, and is homogeneous in composition within a single specimen. Chlorites in ferrogabbro and plagiogranite tend to be deep green, whereas those in metabasalts are pale green. Such differences may be due to differences in  $\text{Fe}_2\text{O}_3$  content and in  $\text{Fe}/(\text{Fe} + \text{Mg})$  ratio. The Sanbagawa chlorites contain about 10 wt.% total Fe as  $\text{Fe}_2\text{O}_3$  (Banno, 1964). The analyzed chlorites range from pychnochlorite to ripidolite through brunsvigite on Hey's (1954) diagram. They are plotted together with pumpellyite and stilpnomelane in terms of  $2\text{Al}-\text{Fe}^*-\text{Mg}$  in Figure 8. All chlorites contain nearly constant Al but show significant variation in  $\text{Fe}/(\text{Fe} + \text{Mg})$  ratio. For pyroxene-bearing assemblages, depending on the other coexisting phases, this ratio in chlorite varies systematically with pyroxene composition from 0.39 to 0.68 as shown in Figure 5.

### *Stilpnomelane*

Stilpnomelane appears only in high  $\text{FeO}^*/\text{MgO}$  metabasites, as brown needles in the matrix. Several analyses are plotted in Figure 8; they contain very high FeO as total Fe and have rather restricted compositions in terms of  $2\text{Al}-\text{Fe}^*-\text{Mg}$ . It may be ferristilpnomelane in composition, but may have been ferrostilpnomelane originally (Brown, 1971). The coexisting chlorite is dark green and has an  $\text{Fe}/(\text{Fe} + \text{Mg})$  ratio of about 0.68 and the coexisting pumpellyite is enriched in Fe content.

## Paragenesis

The petrologic system of metabasites is discussed in terms of the components  $\text{SiO}_2-\text{TiO}_2-\text{Al}_2\text{O}_3-\text{Fe}_2\text{O}_3-\text{FeO}-\text{MgO}-\text{CaO}-\text{Na}_2\text{O}-\text{K}_2\text{O}-\text{H}_2\text{O}-\text{CO}_2$ . Quartz, albite, sphene and phengitic mica are ubiquitous in metabasites; they are treated as excess phases for  $\text{SiO}_2$ ,  $\text{Na}_2\text{O}$ ,  $\text{TiO}_2$  and  $\text{K}_2\text{O}$ , respectively. This simplification reduces the total number of components to five:  $\text{Al}_2\text{O}_3$ ,  $\text{Fe}_2\text{O}_3$ ,  $\text{FeO}$ ,  $\text{MgO}$  and  $\text{CaO}$ , assuming the fluid phase is in excess and consists mainly of  $\text{H}_2\text{O}$  in the calcite-free assemblages. If we fix the chlorite composition at constant  $\text{Fe}/(\text{Fe} + \text{Mg})$ , the system can be further simplified to the four components  $\text{CaO}-\text{Al}_2\text{O}_3-\text{Fe}_2\text{O}_3-(\text{Fe}/\text{Mg})\text{O}$ . The minerals treated here are epidote, chlorite, pumpellyite, actinolite, stilpnomelane, hematite, crossite-riebeckite and Ca-Na pyroxene. The first 6 phases plot within the tetrahedron in Figure 9, but the latter two plot outside. Acmite is plotted at an

Table 2. Representative chemical analyses of metamorphic and relict igneous materials

Mineral	Chl	Ep	Act	Ri	Fum	Px	Chl	Pu	St	Px	Chl	Ep	Act	Pu	Px
Assemblage Sp. No.	E C A Pu Px (Ri) (#1202)						C Pu S Px (#605)				E C A Pu Px (#0512)				
SiO <sub>2</sub>	27.5	36.4	52.1	54.0	35.6	51.8	25.7	35.1	37.3	50.3	25.9	36.7	55.0	36.1	51.5
TiO <sub>2</sub>	0.04	0.19	0.05	0.01	0.07	0.05	0.02	0.05	0.00	0.13	0.00	0.01	0.00	0.02	0.08
Al <sub>2</sub> O <sub>3</sub>	17.4	21.7	1.35	1.99	22.2	1.18	15.1	17.6	12.2	1.07	19.8	21.8	0.69	20.9	3.18
Fe <sub>2</sub> O <sub>3</sub>		15.2		26.8		16.2				34.7		17.0			
FeO	24.3		15.5		9.22		40.4	16.3	35.6		29.1		12.9	11.1	9.05
MnO	0.28	0.09	0.18	0.07	0.13	0.39	0.21	0.01	0.21	0.39	0.49	0.03	0.14	0.06	1.42
MgO	16.3	0.04	14.1	7.50	1.95	7.73	7.06	1.11	7.91	8.27	13.2	0.01	16.1	2.86	10.3
CaO	0.09	22.8	11.5	0.90	22.2	17.6	0.06	21.3	0.43	5.26	0.08	22.9	12.0	22.4	22.2
H <sub>2</sub> O	0.04	0.01	1.15	7.14	0.07	4.24	0.00	0.00	0.06	1.02	0.12	0.04	0.65	0.09	1.36
K <sub>2</sub> O	0.05	0.02	0.09	0.02	0.02	0.04	0.08	0.01	0.26	0.01	0.03	0.00	0.02	0.02	0.03
Total	86.03	96.45	96.02	98.43	91.46	99.23	88.63	91.48	93.97	100.15	88.72	98.49	97.50	93.55	99.12
No. of Oxygen	28	12.5	23	23	24.5	6	28	24.5	22	6	28	12.5	23	24.5	6
Si	5.887	2.971	7.771	7.715	6.007	2.017	5.862	6.160	5.915	1.872	5.513	2.945	7.925	6.025	1.957
Ti	0.006	0.012	0.005	0.001	0.009	0.001	0.004	0.006	0.000	0.004	0.000	0.001	0.003	0.002	
Al	4.393	2.087	0.236	0.336	4.419	0.054	4.066	3.647	2.292	0.047	4.974	2.062	0.118	4.111	0.142
Fe <sup>3+</sup>		0.932		2.886		0.527				0.972		1.026			
Fe <sup>2+</sup>	4.344		1.928		1.302		7.704	2.391	4.728		5.180		1.549	1.561	0.287
Mn	0.051	0.006	0.022	0.008	0.019	0.013	0.041	0.002	0.029	0.012	0.089	0.002	0.017	0.009	0.046
Mg	5.193	0.005	3.130	1.600	1.491	0.448	2.400	0.291	1.872	0.459	4.197	0.001	3.458	0.712	0.581
Ca	0.020	1.994	1.837	0.137	4.013	0.734	0.016	4.012	0.073	0.210	0.018	1.969	1.861	4.000	0.902
Na	0.017	0.001	0.332	1.979	0.024	0.319	0.000	0.001	0.020	0.074	0.050	0.006	0.180	0.028	0.100
K	0.012	0.003	0.016	0.003	0.004	0.002	0.022	0.001	0.052	0.005	0.007	0.000	0.003	0.004	0.002

Mineral	Chl	Act	Ri	Ep	Px	Chl	Ep	Pu	Chl	Pu	Px	Chl	Act	Ep
Assemblage Sp. No.	E C A R H Px (#1611)					E C A Pu (#0105)			E C Pu Px (#2301)			E C A R (#1205)		
SiO <sub>2</sub>	27.3	52.9	52.5	35.7	52.7	27.3	36.2	35.8	27.6	36.5	51.6	28.3	53.0	37.3
TiO <sub>2</sub>	0.04	0.00	0.02	0.18	0.04	0.00	0.34	0.07	0.03	0.05	0.51	0.02	0.06	0.34
Al <sub>2</sub> O <sub>3</sub>	17.4	1.15	1.44	20.2	2.01	18.1	20.4	22.6	18.4	24.8	2.49	15.9	0.91	21.8
Fe <sub>2</sub> O <sub>3</sub>		24.5		17.5	26.2		16.1							15.1
FeO	26.3	17.5				22.9		7.64	18.8	4.96	7.71	22.1	12.7	
MnO	0.48	0.34	0.25	0.13	0.22	0.52	0.15	0.19	0.34	0.12	0.15	0.26	0.20	0.10
MgO	14.6	12.9	3.64	0.43	2.78	16.7	0.24	2.02	19.5	3.00	16.1	17.8	15.5	0.06
CaO	0.13	10.1	8.52	22.5	6.49	1.08	20.9	22.5	0.37	22.6	21.0	0.05	11.9	22.2
H <sub>2</sub> O	0.00	2.25	8.61	0.03	10.2	0.00	0.00	0.00	0.03	0.62	0.10	0.07	1.28	0.00
K <sub>2</sub> O	0.11	0.09	0.01	0.00	0.00	0.02	0.06	0.03	0.11	0.01	0.01	0.12	0.12	0.02
Total	86.36	97.23	99.49	96.87	100.73	86.62	94.39	90.85	85.18	92.66	99.67	84.62	95.67	96.92
No. of Oxygen	28	23	23	12.5	6	28	12.5	24.5	28.0	24.5	6	28	23	12.5
Si	5.890	7.854	7.624	2.935	1.980	5.790	3.015	6.038	5.793	5.946	1.916	6.093	7.830	3.013
Ti	0.006	0.000	0.002	0.011	0.001	0.001	0.021	0.009	0.004	0.006	0.014	0.003	0.006	0.021
Al	0.427	0.200	0.247	1.950	0.089	4.520	2.000	4.496	4.554	4.761	0.109	4.029	0.158	2.078
Fe <sup>3+</sup>			2.679	1.079	0.741		1.008							0.920
Fe <sup>2+</sup>	4.743	2.168				4.049		1.076	3.305	0.674	0.239	3.977	1.571	
Mn	0.088	0.042	0.031	0.009	0.007	0.094	0.011	0.027	0.060	0.017	0.005	0.047	0.025	0.007
Mg	4.697	2.849	0.788	0.076	0.156	5.280	0.030	0.508	6.105	0.727	0.892	5.698	3.420	0.008
Ca	0.030	1.604	1.326	1.576	0.261	0.246	1.870	4.063	0.084	3.938	0.837	0.012	1.880	1.922
Na	0.000	0.647	2.425	0.005	0.739	0.000	0.000	0.000	0.010	0.194	0.007	0.027	0.367	0.000
K	0.029	0.017	0.001	0.000	0.000	0.005	0.006	0.006	0.029	0.001	0.001	0.032	0.022	0.003

infinite point, and solid solution between augite and actinite is shown.

#### Calcite-free and pyroxene-free assemblages

These assemblages contain epidote, chlorite, pumpellyite, actinolite, hematite, crossite-riebeckite, and stilpnomelane and are characteristic for the pumpellyite-actinolite facies. Depending on the bulk rock composition, the assemblages of the two subgroups are plotted in two tetrahedra. For the metabasites with chlorites of Fe/(Fe + Mg) ranging from 0.35–0.68, the mineral paragenesis is shown in Figure 10A, and for the rocks having

chlorites with this ratio above 0.68 in Figure 10B. The latter is characterized by pumpellyite + stilpnomelane, and pumpellyite + riebeckite, which is incompatible with the epidote-chlorite-actinolite plane in Figure 10A. Therefore, at Fe/(Fe + Mg) = 0.68, five phases epidote + chlorite + actinolite + riebeckite + pumpellyite coexist. This 5-phase assemblage is divariant for the five-component system and hence the Fe/(Fe + Mg) of chlorite is a function of temperature and pressure. This ratio increases with increasing temperature as stilpnomelane occurs only in the lower grade part of the Sanbagawa belt, and pumpellyite does not coexist with alkali amphibole in higher grade rocks (Banno, 1964).

Table 2. (cont.)

Mineral	Px						Chl					Act			
	Chl	Ep	Ri	Sti	(core)	(rim)	Chl	Ep	Ri	Sti	Px	Chl	Ep	Act	Px
Assemblage Sp. No.	E C Px Ht R S (#2201)						E C S R Px (#2007)					E C A Px (#1811)			
SiO <sub>2</sub>	24.0	36.5	50.7	44.7	53.2	52.3	30.7	36.4	50.8	43.4	50.9	26.2	40.9	52.3	50.3
TiO <sub>2</sub>	0.02	0.02	0.30	0.01	0.08	0.11	0.00	0.07	0.10	0.02	0.12	0.00	0.00	0.61	0.00
Al <sub>2</sub> O <sub>3</sub>	18.4	23.3	4.44	6.15	6.25	6.78	16.8	20.8	4.09	6.01	2.52	17.5	18.7	2.34	1.39
Fe <sub>2</sub> O <sub>3</sub>		13.2	29.6		24.7	23.7		15.1	25.0				13.8		
FeO	34.6			30.6			29.0			30.1	15.2	26.6		13.2	15.3
MnO	0.29	0.17	0.15	0.67	0.07	0.08	0.34	0.17	0.14	0.82	0.18	0.22	0.03	0.19	0.33
MgO	8.86	0.02	4.97	4.39	0.70	0.69	12.8	0.00	6.14	5.89	9.50	14.6	0.05	15.3	8.27
CaO	0.00	23.0	2.20	0.23	2.09	1.97	0.00	22.3	4.73	0.00	15.0	0.09	22.8	11.5	21.7
Na <sub>2</sub> O	0.00	0.04	7.01	0.13	13.7	13.2	0.00	0.01	6.35	0.04	5.90	0.07	0.35	0.73	3.75
K <sub>2</sub> O	0.01	0.02	0.11	0.83	0.02	0.02	0.01	0.02	0.03	1.57	0.02	0.01	0.03	0.11	0.00
Total	86.18	96.27	99.48	87.71	100.81	98.85	89.65	94.87	97.38	87.85	99.34	85.29	96.66	96.28	101.06
No. of Oxygen	28.0	12.5	23.0	22	6	6	28.0	12.5	23	22		28	12.5	23	6
Si	5.466	2.963	7.295	7.343	1.970	1.967	6.383	3.018	7.407	7.173	1.967	5.740	3.290	7.671	1.943
Ti	0.003	0.001	0.032	0.002	0.002	0.003	0.000	0.005	0.011	0.003	0.003	0.000	0.000	0.067	0.000
Al	4.938	2.230	0.752	1.190	0.273	0.301	4.110	2.030	0.703	0.169	0.114	4.531	1.771	0.404	0.063
Fe <sup>3+</sup>		0.805	3.203		0.688	0.670		0.943	2.746				0.838		
Fe <sup>2+</sup>	6.596			4.208			5.049			4.159	0.491	4.873		0.619	0.493
Mn	0.056	0.012	0.018	0.093	0.002	0.003	0.060	0.012	0.017	0.114	0.006	0.042	0.002	0.024	0.011
Mg	3.008	0.002	1.066	1.076	0.039	0.038	3.967	0.000	1.334	1.449	0.547	4.778	0.006	3.351	0.476
Ca	0.000	2.001	0.339	0.041	0.083	0.080	0.000	1.985	0.739	0.000	0.622	0.020	1.970	1.809	0.900
Na	0.000	0.006	1.957	0.042	0.982	0.964	0.000	0.001	1.796	0.014	0.442	0.031	0.055	0.206	0.281
K	0.002	0.002	0.020	0.173	0.001	0.001	0.003	0.002	0.005	0.330	0.001	0.003	0.003	0.020	0.000

Mineral	Chl					Act					Relict Augite	
	Chl	Act	Ri	Pu	Sti	Chl	Pu	Act	Ri*	Px	(#601)	(#602)
Assemblage Sp. No.	R A C Pu S (#604)					C A Pu Px (#607)						
SiO <sub>2</sub>	29.1	51.0	51.5	35.2	47.3	31.7	34.6	49.4	51.7	47.5	51.4	48.9
TiO <sub>2</sub>	0.05	0.00	0.05	0.10	0.00	0.00	0.09	0.04	0.05	0.10	0.38	2.16
Al <sub>2</sub> O <sub>3</sub>	12.8	2.87	2.92	20.4	8.02	11.5	13.7	1.72	2.41	2.32	2.15	7.53
Fe <sub>2</sub> O <sub>3</sub>			31.5						31.9			
Cr <sub>2</sub> O <sub>3</sub>											1.07	0.00
FeO	35.3	24.9		12.4	28.6	35.7	19.8	28.9		35.1	6.39	11.6
MnO	0.13	0.12	0.05	1.80	0.29	0.14	0.03	0.23	0.07	0.15	0.17	0.36
MgO	8.85	5.57	4.07	1.80	3.34	9.98	1.19	5.24	5.57	1.74	17.0	12.3
CaO	0.65	10.5	2.02	20.8	0.31	0.53	21.2	9.27	3.18	10.7	20.8	17.2
Na <sub>2</sub> O	0.13	3.81	6.22	0.03	1.68	0.09	0.03	1.94	5.60	1.00	0.11	0.51
K <sub>2</sub> O	0.03	0.10	0.02	0.02	1.65	0.05	0.00	0.08	0.01	0.10	0.00	0.00
Total	87.04	98.87	98.35	90.82	91.19	89.69	90.64	96.82	100.49	98.71	99.47	100.56
No. of Oxygen	28	23	23	24.5	22	28	24.5	23	23	6	6	6
Si	6.536	7.756	7.495	6.066	7.386	6.875	6.298	7.788	7.386	1.982	1.907	1.816
Ti	0.008	0.000	0.006	0.014	0.000	0.00	0.012	0.004	0.006	0.003	0.011	0.060
Al	3.401	0.514	0.500	4.150	1.475	2.930	2.939	0.319	0.406	0.114	0.094	0.330
Fe <sup>3+</sup>			3.445						3.432			
Fe <sup>2+</sup>	6.629	3.158		1.791	3.731	6.468	3.006	3.807		1.226	0.031	0.000
Mn	0.025	0.015	0.006	0.011	0.038	0.026	0.005	0.031	0.009	0.005	0.005	0.011
Mg	2.966	1.262	0.882	0.462	0.777	3.224	0.324	1.230	1.187	0.108	0.941	0.680
Ca	0.157	1.711	0.315	3.846	0.052	0.122	4.133	1.565	0.487	0.477	0.828	0.685
Na	0.058	1.123	1.754	0.009	0.509	0.039	0.011	0.594	0.551	0.081	0.008	0.037
K	0.010	0.019	0.004	0.003	0.328	0.013	0.000	0.016	0.002	0.005	0.000	0.000

\* Ri is completely surrounded by actinolite.

### Calcite-free and pyroxene-bearing assemblages

This group includes the assemblage pyroxene + chlorite, which is incompatible with the topology in Figures 10A and B of the above group. As shown in Figure 4, compositions of pyroxene and chlorite vary according to mineral assemblage. With increasing acmite mol% in pyroxene, the coexisting chlorites change composition from  $Fe/(Fe + Mg) = 0.35$  to 0.68. For chlorite with  $Fe/(Fe + Mg)$  greater than 0.68, the assemblage pyroxene + chlorite is not stable.

Paragenetic relations for rocks with chlorite of  $X_{Fe}$

ranging from 0.35 to 0.68 are shown in Figure 10C, and are projected from chlorite onto a plane perpendicular to the 2Al-Ca-FM plane and 80° inclined to the Ca-2Al join according to Figure 9. Mineral assemblages of the pumpellyite-actinolite facies are shown. Depending on the bulk rock  $Fe^{3+}/Al$  ratio, assemblages of pumpellyite-actinolite, epidote-pumpellyite-actinolite, epidote-actinolite, epidote-actinolite-riebeckite, hematite-epidote-riebeckite and hematite-riebeckite may occur. Superimposed on these mineral compatibilities are the compositions of pyroxene solid solution between augite-acmite at constant jadeite end-member of 20 mol%. Because the

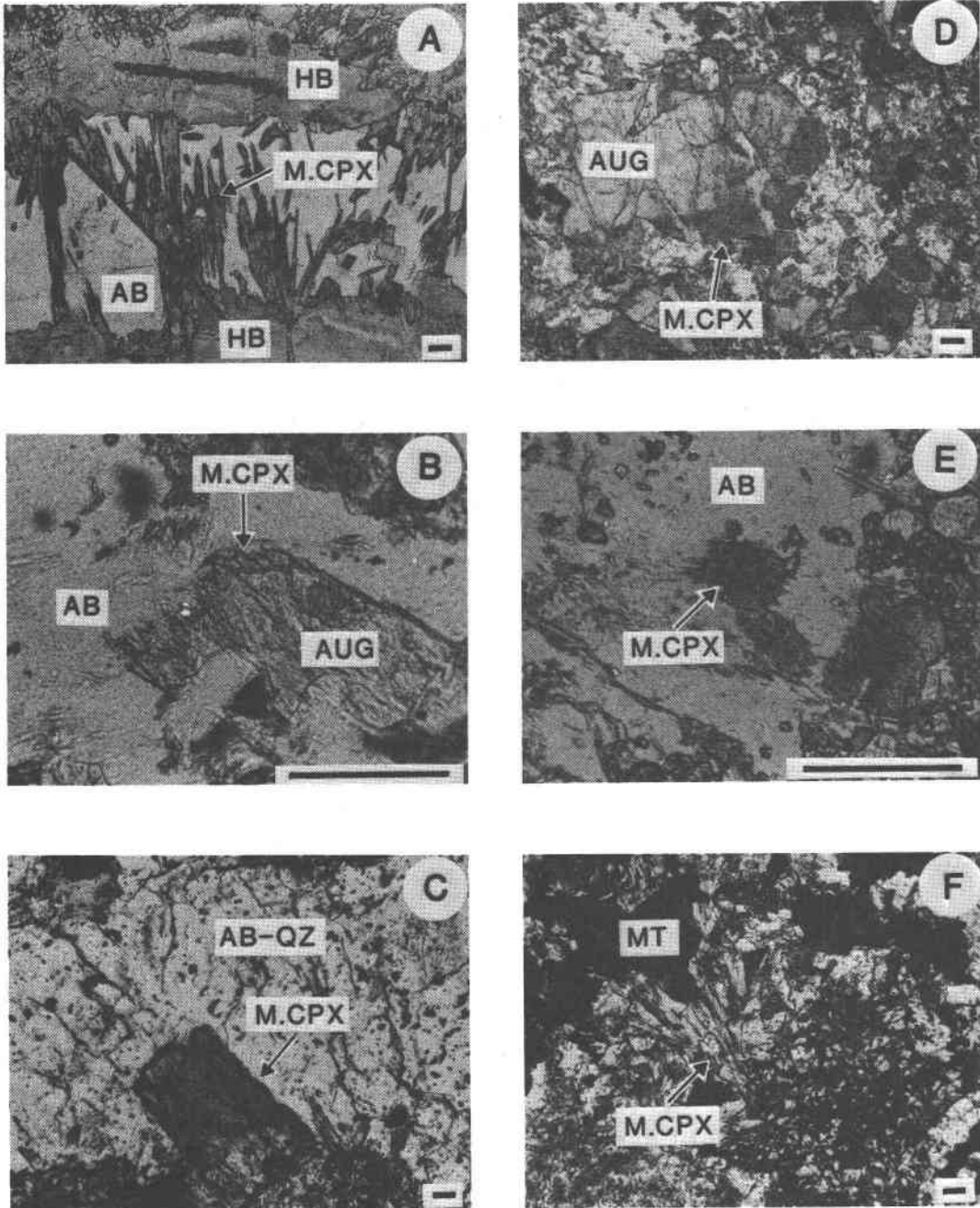


Fig. 3. Photomicrographs show the occurrence of some metamorphic pyroxenes in metabasalts from the study area. Scale bar is 0.1 mm. Abbreviations are Hb: hornblende; Ab: albite; M-CPX: metamorphic clinopyroxene; Aug: relict augite; MT: metamorphic magnetite. A. Acicular needles of metamorphic Ca-Na pyroxenes growing into albite. B. Thin rims of Ca-Na pyroxenes growing epitaxially along margin of relict augite. C. Metamorphic zoned Ca-Na pyroxenes growing into an albite + minor quartz vein. The detailed compositional profile is shown in Fig. 11. D. Metamorphic pyroxene replacing the relict augites along margins or irregular cracks. E. Discrete metamorphic pyroxene grain within albite together with phengitic mica and chlorite. F. Fan-shaped metamorphic pyroxenes intergrown with metamorphic magnetite.

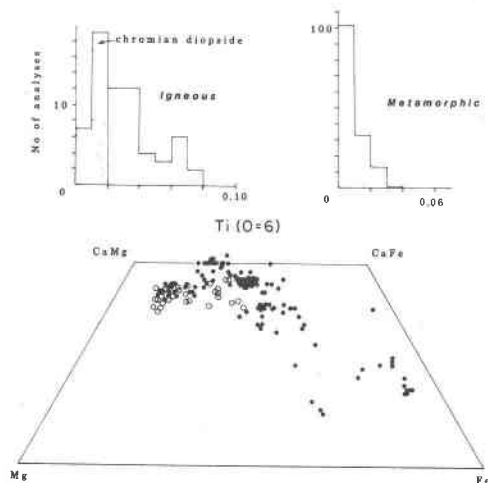


Fig. 4. Contrast in chemical compositions between metamorphic (closed circles) and igneous (open circles) pyroxenes of the metabasites in the study area.

augite-acmite solid solution is incompatible with the pumpellyite-actinolite assemblages, six reactions are apparent from the paragenetic relations and are written below:

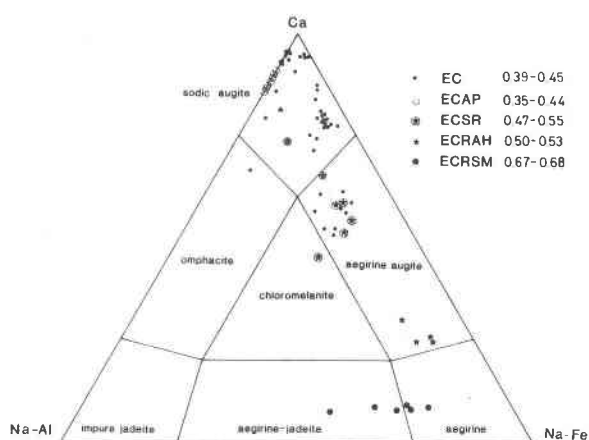
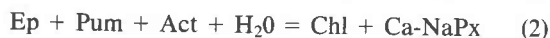
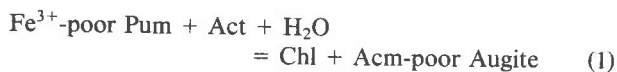


Fig. 5. Compositions of metamorphic pyroxenes plotted in a ternary diagram of Ca (Di + Hd) - Na-Al (jadeite) - Na-Fe (acmite) system. Abbreviations: E = epidote, C = chlorite, A = actinolite, P = pumpellyite, S = stilpnomelane, R = riebeckite, H = hematite and M = magnetite. Those numbers shown on the right top corner are the Fe/(Fe + Mg) ranges of the coexisting chlorites.

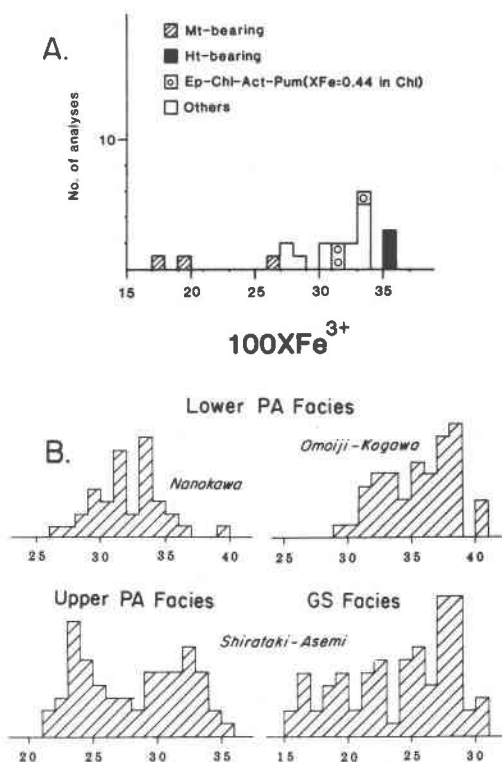


Fig. 6. A. Compositions of epidotes in various assemblages from the study area. B. Histograms showing compositions of epidotes of a buffered assemblage epidote-chlorite (Fe/(Fe + Mg) = 0.40-0.45) - pumpellyite-actinolite-quartz in lower and upper pumpellyite-actinolite and greenschist facies metabasites (data are from Aiba, 1980, Nakajima et al., 1977 and Nakajima, 1982).

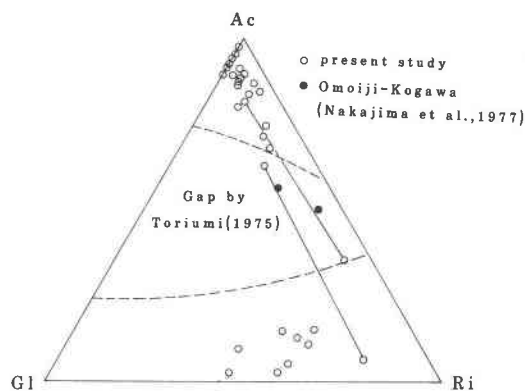
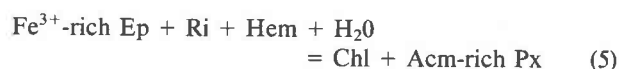


Fig. 7. Compositions of amphiboles in a ternary diagram of actinolite (Ac), glaucophane (Gl) and riebeckite (Ri) components. Also shown is the composition gap by Toriumi (1975).

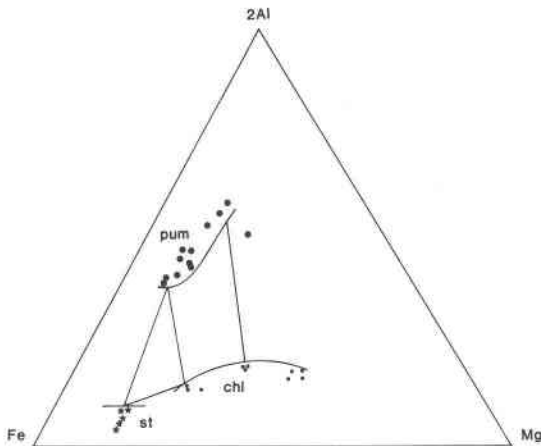


Fig. 8. Compositions of pumpellyite (pum) (large solid circle), chlorite (chl) (small solid circle) and stilpnomelane (st) (solid star) plotted on a ternary diagram of 2 Al-Fe\* (total Fe as FeO)-Mg. Coexisting compositions for pumpellyite-chlorite and pumpellyite-chlorite-stilpnomelane are shown by tie lines.

From equations (1) to (6), pyroxene changes composition from augite to acmitic augite. This relationship is consistent with the variation of clinopyroxene composition shown in Figure 5. Because  $H_2O$  is required for the formation of the pyroxene-bearing assemblages, pyroxene-chlorite assemblages are stable at lower temperatures than those of the pumpellyite-actinolite compatibilities.

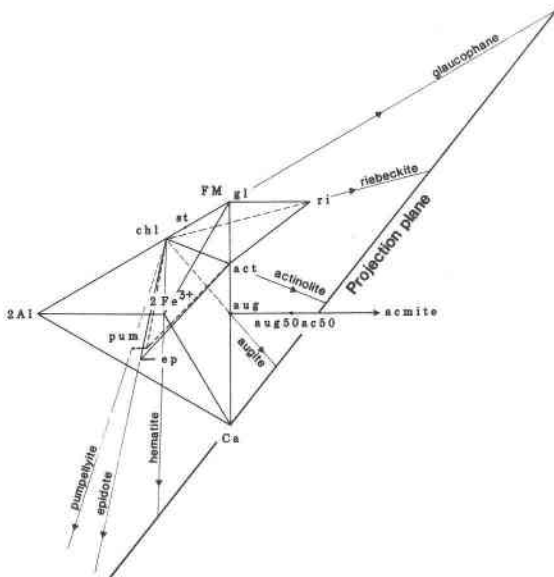


Fig. 9. Compositional relations of chlorite (chl), stilpnomelane (st), pumpellyite (pum), epidote (ep), actinolite (act), glaucophane (gl), riebeckite (ri), augite (aug) and acmite (ac) in a tetrahedron of 2 Al - 2 Fe<sup>3+</sup> - Ca - FM components. A projection plane perpendicular to the 2Al-Ca - FM plane and about 80° inclined to the Ca-2Al join is shown.

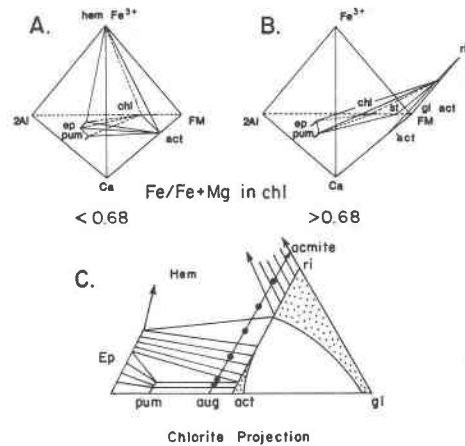


Fig. 10. Mineral parageneses of metabasites from the study area and chlorite projection to show the pyroxene-forming reaction: A. Metabasite assemblages for the rocks with chlorite of Fe/(Fe + Mg) ratio ranging from 0.35–0.68; B. For rocks with chlorite of Fe/(Fe + Mg) ratio greater than 0.68; C. Incompatible pyroxene-bearing assemblages with those in A on a chlorite-projection diagram showing (a) the six reactions described in the text, and (b) systematic variation of pyroxene composition along the join augite-acmite with variation in reactions.

In the northern, higher pumpellyite-actinolite facies rocks, the pyroxene-bearing assemblage is extremely rare. None was reported by Banno (1964) and only one pyroxene-stilpnomelane-bearing metabasite has been described by Otsuki (1980). By contrast, to the southwest of the study area, pyroxene + chlorite assemblages have been described by Iwasaki (1963) and Aiba (1980). From the previous and present studies, it is concluded that the pyroxene-bearing assemblage is stable at the lower grade part of the pumpellyite-actinolite facies, with metamorphic conditions roughly corresponding to those of the narrow region of the present study area. The pyroxene-bearing and pyroxene-free assemblages are randomly distributed through the area, suggesting local differences in the activity of  $H_2O$ ; high  $a_{H_2O}$  favored the occurrence of the pyroxene + chlorite assemblage.

#### Calcite-bearing and pyroxene-free assemblages

Rocks with high FeO\*/MgO may contain a calcite-stilpnomelane assemblage. For lower FeO\*/MgO rocks, calcite-chlorite-riebeckite assemblages occur, and they are incompatible with actinolite-epidote or actinolite-pumpellyite as shown in Figure 10A. These relations suggest that the appearance of calcite is controlled by local increase of  $X_{CO_2}$  in the fluid. The value of  $X_{CO_2}$  in the fluid might be lower than 0.02 at about 300°C, judged from the common occurrence of sphene rather than rutile-calcite-quartz (Ernst, 1972). However, it should be emphasized that only about 2% of the metabasites contain carbonate-bearing assemblages. Therefore, it is reasonable to conclude the fluid phase present during the

pumpellyite-actinolite facies metamorphism of basaltic rocks from the study area was highly aqueous.

### Discussion

#### *P-T path of Sanbagawa metamorphism deduced from zoning of clinopyroxene*

Most examined Ca-Na pyroxenes exhibit progressive zoning with higher jadeite content towards the rim. A few grains contain a thin film of less jadeitic pyroxene at the outermost margin. One example (SP1811) is shown in Figure 11. The pyroxene, 0.8 x 1.0 mm in size, grew into an albite-quartz vein. Fifty analyses for 9 elements were completed for this crystal, and the jadeite mol% of the analyses are shown in Figure 11. Jadeite component increases from 0.5–2.4% up to 5.3% in the core region, and decreases gradually towards the rim. The outermost rim ranges from 0.4 to 2.3%. Such a distribution pattern shows a progressive zoning for the core followed by a retrogressive one for the rim, and is not common in Sanbagawa metabasites. It may be related to the vein-forming process whereby metamorphic recrystallization advanced rapidly due to sufficient material migration through veins. The same sample contains groundmass clinopyroxene grains with about 19 mol% jadeite. These compositional variations among clinopyroxene crystals within a single sample probably indicate local equilibrium. Although local equilibrium may have prevailed during recrystallization, as discussed before, the systematic difference in pyroxene composition suggests that the mineral assemblages may have approached equilibrium.

The jadeitic pyroxene-albite-quartz sliding equilibrium as shown in Figure 12 is independent of the presence or absence of a fluid phase. Thus we are able to estimate the *P-T* path of the Sanbagawa metamorphism without knowing the exact values of  $a_{H_2O}$ . The diopside-acmite-jadeite

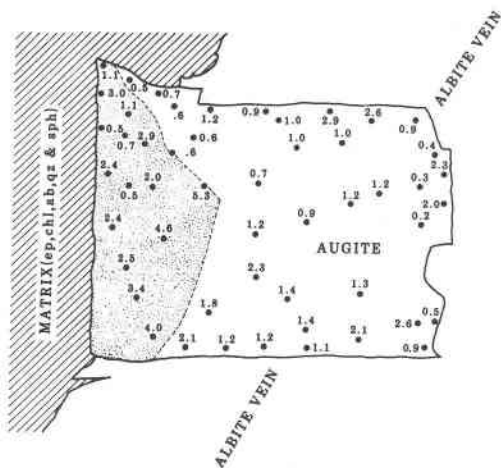


Fig. 11. Compositions of a zoned pyroxene crystal grown into an albite-quartz vein as expressed by mol% of jadeite component (see Fig. 3C for the occurrence).

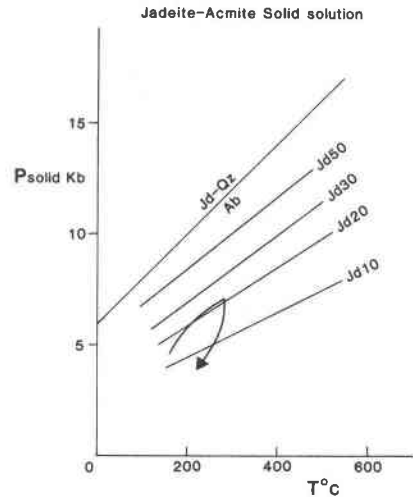


Fig. 12. The *P-T* path of the Sanbagawa metamorphism deduced from zoned pyroxene coexisting with albite and quartz.

system, however, includes two miscibility regions between omphacite (*P2/n*)-augite (*C2/c*) and omphacite-jadeite (*C2/c*) (e.g., Carpenter, 1980) and the ideal solution model of Essene and Fyfe (1967) is not valid under the conditions of low-grade metamorphism. However, immiscibility regions are closed towards the augite end-member under the lawsonite grade of jadeite-glaucophane type metamorphic belts (Carpenter, 1980; Okay, 1980). It is valid to discuss a *P-T* path, using pyroxene sliding equilibria only in the miscibility region. Figure 5 shows the compositional range of Ca-Na pyroxenes in the study area, and covers only the miscibility region.

The possible *P-T* path for the Sanbagawa metamorphism is shown in Figure 12 together with the equilibrium line of jadeite + quartz + albite line (Birch and Le Comte, 1960) and calculated isopleths of 30%, 20% and 10% jadeite end-member by Essene and Fyfe (1967). Chemical zoning shown in Figure 11 indicates that initially both pressure and temperature increased, then temperature increased with or without an accompanying pressure drop, and finally both *P* and *T* decreased. The *P-T* trajectory shown in Figure 12 is in good agreement with those estimated from garnet-chlorite-biotite equilibria by Higashino (1975) and amphibole zoning by Otsuki (1980) for the Sanbagawa metamorphism.

#### *Distribution of metamorphic facies in the Sanbagawa belt in Shikoku*

The metamorphic grade in central Shikoku generally decreases from north to south. The highest grade metabasites contain albite-oligoclase-hornblende-epidote (Enami, 1981) of the amphibolite facies. With decreasing grade towards the south, the metabasites successively exhibit mineral assemblages of the albite-epidote amphibolite, greenschist, pumpellyite-actinolite and finally prehnite-pumpellyite facies (Hashimoto et al., 1970; Banno,

1977). Figure 1 shows the distribution of metamorphic facies in the lower grade part of the Sanbagawa belt in Shikoku through comparison of the metamorphic grade of the study area to those of surrounding areas.

Banno and his coworkers (Kurata and Banno, 1974; Higashino, 1975; Nakajima et al., 1977; Nakajima, 1982) have defined several continuous reactions to relate such changes in mineral assemblages according to parageneses and compositions of particular minerals of the buffered assemblages. For example, Nakajima et al. (1977) and Nakajima (1982) delineated metamorphic grade using the composition of epidote in buffered assemblage, epidote-chlorite-pumpellyite-actinolite. The  $X_{Fe}$  of chlorite is fixed at 0.45–0.50. Frequency distribution diagrams of epidote composition show a systematic increase in Al content of epidote with increasing temperature (Nakajima, 1982). Compositions of the analyzed epidotes from PS 31 to PS 34 (Fig. 5), corresponding to the epidote compositions of the lower pumpellyite-actinolite facies and similar to those in metabasites from Omoiji-Kogawa (Nakajima, 1982) and from the Chichibu belt (Aiba, 1980, 1982). The  $Fe^*/Al$  ratio of pumpellyite in the same assemblage has also been used to define the metamorphic grade by Aiba, (1980, 1982); their results ( $Fe^*/Al$  atomic ratio = 24.0 ~ 32.6) are comparable to those in the above two districts.

Figure 13 plots the partition coefficient  $K_{D_{pump-chl}}^{Mn-Mg}$  from the upper pumpellyite-actinolite zone (Otsuki, 1980) and lower pumpellyite-actinolite zone (Nakajima et al., 1977; Aiba, 1980; Nakajima, 1982). The  $K_{D}$ 's of the upper pumpellyite-actinolite zone range from 7 to 10, whereas those in the lower pumpellyite-actinolite zone vary from 3 to 6. The  $K_{D}$ 's for pumpellyite/chlorite pairs from the study area range from 0.9 to 5 and indicate again the lower pumpellyite-actinolite facies. It is thus concluded that the present study area, where metamorphic Ca-Na

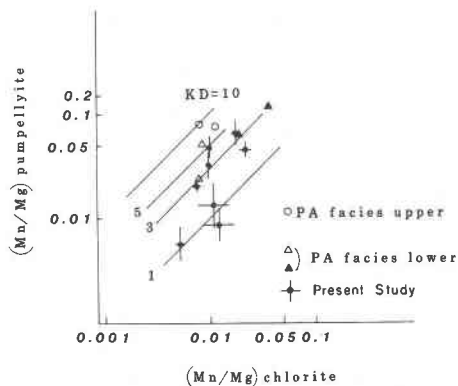


Fig. 13. Mn-Mg partition coefficients between actinolite and chlorite from upper and lower pumpellyite-actinolite facies of the Sanbagawa metamorphic belt. Data for upper and lower pumpellyite-actinolite facies are from Aiba (1980), Nakajima et al. (1977) and Nakajima (1982).

pyroxenes occur, corresponds to lower pumpellyite-actinolite facies.

#### Pumpellyite-actinolite facies

Hashimoto (1966) proposed that the pumpellyite-actinolite facies is an independent facies between the prehnite-pumpellyite metagreywacke and greenschist facies on the lower pressure side, and between the glaucophane schist and greenschist facies on the high-pressure side. This suggestion has been accepted by Seki (1969), Coombs (1971) and others.

Nitsch (1971) experimentally determined the stability limit of epidote + chlorite + actinolite + pumpellyite + quartz + fluid, which occupies a wedge-shaped  $P$ - $T$  space. The high- $T$  and low- $T$  sides are bounded, respectively, by the reactions: pumpellyite + chlorite = epidote + actinolite + fluid, and prehnite + chlorite + fluid = pumpellyite + actinolite. His experiments, however, were conducted using natural minerals as starting material, and the determined  $P$ - $T$  lines for the above reactions thus are not univariant.

As described earlier, metabasite stability relations can be simplified to a five-component system with excess quartz, albite and fluid (e.g., Zen, 1974; Banno, 1977). The high- $T$  reaction of Nitsch is, therefore, trivariant. At a given  $Fe/(Fe + Mg)$  in the system, the reaction has been treated as divariant by Nakajima et al. (1977) and Nakajima (1982). Hence, the epidote composition varies continuously in  $P$ - $T$  space. In the Sanbagawa belt, the boundary between the pumpellyite-actinolite and greenschist facies is defined by the disappearance of pumpellyite, which may coincide with epidote of  $PS = 15$  for the basaltic system (Nakajima, 1982). In other words, the substitution of Al by  $Fe^{3+}$  remarkably affects the pumpellyite-consuming reaction. They calculated the effect of  $Fe_2O_3$  on the  $P$ - $T$  position of the reaction, and their results indicate that equilibrium occurs  $115^\circ C$  lower for the  $Fe_2O_3$ -saturated condition than for the  $Fe_2O_3$ -free system. The  $Fe^{2+}/Mg$  substitution in actinolite and chlorite might also significantly affect this sliding equilibrium as suggested by their partition coefficients, although the details have not been investigated.

Nakajima et al. (1977) proposed subdivision of the pumpellyite-actinolite facies by the discontinuous reaction: epidote ( $PS = 33$ ) + actinolite + chlorite ( $Fe/(Fe + Mg) = 0.45 - 0.50$ ) +  $H_2O =$  pumpellyite + hematite. The lower- $T$  subfacies is characterized by the metabasite assemblages pumpellyite + hematite + actinolite or pumpellyite + hematite + epidote with excess chlorite, quartz and fluid; epidote cannot coexist with actinolite. Aiba (1982) has, subsequently, confirmed the occurrence of these assemblages in the lower grade part of the Sanbagawa belt, where Iwasaki (1963) and Aiba (1980) also described a Ca-Na pyroxene-chlorite assemblage in some metabasites.

In the previous sections, the Ca-Na pyroxene-chlorite assemblage is shown to be incompatible with a pumpel-

lyite-actinolite assemblage in some metabasites. It occurs in rocks which have been metamorphosed at lower pumpellyite-actinolite facies or at conditions close to those of the discontinuous reaction proposed by Nakajima et al. (1977). This relationship suggests that the low-*T* boundary of the pumpellyite-actinolite facies could also be defined by a reaction different from those proposed by Hashimoto (1966), Nitsch (1971) and Seki (1971).

#### Stability field of Ca-Na pyroxene + chlorite + pumpellyite

The assemblage augite + chlorite appears to be stable at the *P-T* conditions defined near the above discontinuous reaction by Nakajima et al. (1977), and it can be used to subdivide the pumpellyite-actinolite facies. Immediately north of the study area occur the characteristic pumpellyite-actinolite facies assemblages. To the south of the study area, augitic to acmitic pyroxenes have been found by Iwasaki (1963) and Aiba (1980). Further south, the prehnite-pumpellyite zone is developed (Hashimoto et al., 1970). Therefore, the augite + chlorite assemblage is stable at restricted conditions between those of the pumpellyite-actinolite and the prehnite-pumpellyite zones. Augite-chlorite zones have not been recognized between the prehnite-pumpellyite and pumpellyite-actinolite zones from either higher or lower *P/T* facies series, such as New Zealand (Coombs, 1971; Kawachi, 1975; Coombs et al., 1976), the Appalachians (Zen, 1974), and New Caledonia (Black, 1977; Brothers, 1974). Appearance of augite with chlorite may be restricted to metabasites of the high-pressure intermediate facies series.

At constant  $Fe^{3+}/Al$  ( $PS = 33$ ) in epidote and  $Fe/(Fe + Mg)$  (0.45) in chlorite, the topologic relationships of epidote, prehnite, lawsonite, pumpellyite, actinolite and augite in low-grade metabasite in a ternary ACF system are constructed. As chlorite is ubiquitous in metabasites, compositions of all these Ca-Al silicates are projected from the Sanbagawa chlorite  $(Mg,Fe)_5Al_2Si_4O_{15}(OH)_{12}$  onto the pseudo-binary join A-C. There are 4 univariant lines radiating from each invariant point for the pseudo-binary system. However, for clarity, some invariant points are shown with only 3 univariant lines. Among 15 invariant points ( ${}_6C_4 = 15$ ), four are relevant to our discussion on the augite stability; they are shown in Figure 14. The first invariant point [Lw, Aug], from which radiate four univariant lines, was estimated by Nitsch (1971) to occur at 2.5 Kbar and 350°C.

One of these lines is the reaction  $Pr + Chl + F = Act + Pum$ , which has a negative slope and defines the boundary between the prehnite-pumpellyite and pumpellyite-actinolite facies. Mineral parageneses in New Zealand from the prehnite-pumpellyite zone grading directly to the pumpellyite-actinolite zone without passing through the augite zone, can be defined by the above reaction. At higher pressure, this reaction is terminated at another invariant point [Ep, Lw], from which radiates another three reactions; two of them extend towards higher

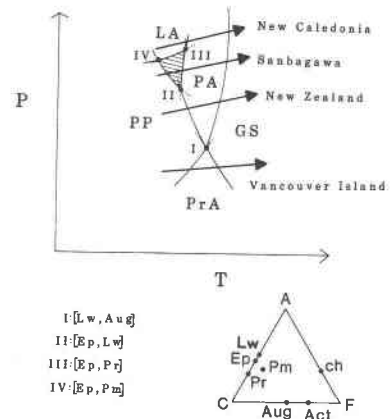


Fig. 14. Possible *P-T* stability field (shaded area) for the augite-chlorite-pumpellyite assemblage in basaltic ACF system. The phase relations are constructed for a pseudobinary system projected from constant chlorite composition. Arrows indicate the *P-T* trajectories for different metamorphic facies series. For stability relations among the prehnite-pumpellyite, pumpellyite-actinolite, prehnite-actinolite and greenschist facies see Liou et al. (1985).

pressures. These two reactions, as shown in Figure 14, define successive zones of pumpellyite + prehnite, augite + pumpellyite, and pumpellyite + actinolite with increasing grade. The boundary between the prehnite-pumpellyite and augite + pumpellyite zones is defined by a reaction: prehnite + actinolite +  $H_2O =$  augite + chlorite with a negative steep *P-T* slope. The boundary between the augite-pumpellyite and pumpellyite-actinolite zones is defined by a dehydration reaction: augite + chlorite = pumpellyite + actinolite +  $H_2O$  with a positive slope.

In New Caledonia, a metamorphic zone characterized by lawsonite-actinolite without augite develops on the lower-*T* side of the pumpellyite-actinolite zone (Brothers, 1974). Therefore, an invariant point [Ep, Pr] might be stable between 6 kbar for the Sanbagawa metamorphism (Toriumi, 1975) and about 8 kbar in New Caledonia (Brown, 1977; Brothers and Yokoyama, 1982). Radiating from the invariant point is the invariant solid-solid reaction: lawsonite + actinolite = augite + chlorite, which defines the high-pressure limit of the augite + pumpellyite zone. A similar stability field of augite + chlorite in the lower grade part of the Kanto Mountains, has been recently deduced from a complete solution of the ACF system with 7 phases: augite, chlorite, pumpellyite, glaucophane, actinolite, lawsonite and epidote (Hirajima, 1983).

It is apparent from Figure 14 that the small *P-T* space, in which the augite + chlorite + pumpellyite assemblage is stable, exhibits a wedge shape with decreasing pressure. This assemblage appears only in the low-grade part, between the prehnite-pumpellyite and pumpellyite-actinolite zones, of the high-pressure intermediate facies series.

### Conclusions

Several conclusions are deduced from the petrological-mineralogical study of some low-grade metabasites described in the previous sections. They are listed below:

1. Minor amounts of Ca-Na clinopyroxenes occur as minute fibrous crystals, metasomatic replacements as well as thin rims around primary augites in some metabasites between the prehnite-pumpellyite and pumpellyite-actinolite facies.

2. The Ca-Na clinopyroxenes are stable with chlorite + pumpellyite  $\pm$  epidote  $\pm$  actinolite  $\pm$  stilpnomelane  $\pm$  crossite  $\pm$  hematite  $\pm$  magnetite in these metabasites.

3. The Ca-Na clinopyroxenes are very heterogeneous in composition and contain much lower Cr<sub>2</sub>O<sub>3</sub>, TiO<sub>2</sub> wt.% and OPX mol% than the relict primary augites.

4. The Ca-Na clinopyroxenes vary in composition systematically with their coexisting mineralogy; those in pumpellyite-bearing assemblages contain a very low acmite component (Ac<sub>0</sub>Aug<sub>80</sub>Jd<sub>20</sub>), and increase through Ac<sub>25</sub>Aug<sub>55</sub>Jd<sub>20</sub> in the crossite-bearing and Ac<sub>60</sub>Aug<sub>25</sub>Jd<sub>15</sub> in the hematite-bearing, and to Ac<sub>65</sub>Aug<sub>10</sub>Jd<sub>25</sub> aegirine in the magnetite-bearing assemblage.

5. Such a systematic change in pyroxene composition is explained by a series of reactions deduced from (1) difference in paragenesis and compositions of minerals in the pumpellyite-actinolite and prehnite-pumpellyite facies metamafics, and (2) topologic relations of phases in a basaltic ACF system.

6. Composition of chlorite and epidote and Mn-Mg distribution between pumpellyite and chlorite together with field relations suggest that the clinopyroxene-bearing metabasites were recrystallized at *P-T* conditions between the prehnite-pumpellyite and pumpellyite-actinolite facies.

7. Stability of the augite-chlorite-pumpellyite assemblage falls within a wedge-shaped *P-T* field that is bounded by a high-*T* reaction augite + chlorite = pumpellyite + actinolite + H<sub>2</sub>O and a low-*T* reaction prehnite + actinolite + H<sub>2</sub>O = augite + chlorite.

### Acknowledgments

The analytical work was completed at Kanazawa University under the guidance of Professor S. Banno. Discussions with S. Banno, T. Hirajima, K. Aiba and T. Nakajima are most helpful. The manuscript was prepared at Stanford where the senior author is a post doctoral research fellow supported by NSF EAR82-04298. We wish to thank Mary Keskinen, Peter Schiffman and W. G. Ernst for critical review of this manuscript.

### References

- Aiba, K. (1980) Sanbagawa metamorphism of the northern part of the Chichibu belt in western central Shikoku. MS Thesis, Kanazawa Univ.
- Aiba, K. (1982) Sanbagawa metamorphism of the Nakatsu-Nanokawa district, the northern subbelt of the Chichibu belt in western central Shikoku. *Journal of Geological Society of Japan*, 88, 875-885.
- Banno, S. (1959) Aegirine augites from crystalline schists in Sikoku. *Journal of Geological Society of Japan*, 65, 652-657.
- Banno, S. (1964) Petrologic studies on Sanbagawa crystalline schists in the Bessi-Ino district, central Shikoku, Japan. *Journal of Faculty Science, University of Tokyo, Sec. II*, 4, 203-319.
- Banno, S. (1977) Mineral facies of the Sanbagawa metamorphic belt. In K. Hide, Ed., *Sanbagawa Belt*, p. 97-106.
- Banno, S., Higashino, T., Otsuki, M., Itaya, T. and Nakajima, T. (1978) Thermal structure of the Sanbagawa metamorphic belt in central Shikoku. *Journal of Physics of Earth*, 26, 345-356.
- Birch, F. and LeComte, P. (1960) Temperature-pressure plane for albite composition. *American Journal of Science*, 258, 209-217.
- Bird, D. K., Schiffman, P., Elders, W. A. and Williams, A. E. (1984) Calc-silicate mineralization in the Cerro Prieto geothermal field, Baja California, Mexico, compared with other geothermal systems. *Economic Geology*, 79, 671-695.
- Black, P. M. (1977) Regional high-pressure metamorphism in New Caledonia: phase equilibria in the Quegoa district. *Tectonophysics*, 43, 89-107.
- Brothers, R. N. (1974) High-pressure schists in northern New Caledonia. *Contributions to Mineralogy and Petrology*, 46, 109-127.
- Brothers, R. N., and Yokoyama, K. (1982) Comparison of the high-pressure schist belts of New Caledonia and Sanbagawa, Japan. *Contributions to Mineralogy and Petrology*, 79, 219-229.
- Brown, E. H. (1971) Phase relations of biotite and stilpnomelene in the greenschist facies. *Contributions to Mineralogy and Petrology*, 31, 275-299.
- Brown, E. H. (1977) Phase equilibria among pumpellyite, lawsonite, epidote and associated minerals in low grade metamorphic rocks. *Contributions to Mineralogy and Petrology*, 64, 123-135.
- Carpenter, M. A. (1980) Mechanisms of exsolution in sodic pyroxenes. *Contributions to Mineralogy and Petrology*, 71, 289-300.
- Cavarretta, G., Gianelli, G., and Puxeddu, M. (1982) Formation of authigenic minerals and their use as indicators of chemico-physical parameters of the fluid in the Larderello-Travale geothermal field. *Economic Geology*, 77, 1071-1084.
- Coombs, D. S. (1971) Present status of the zeolite facies. *Molecular Sieve Zeolites-1*, in *Advances in Chemistry series*, No. 11, American Chemical Society, 317-327.
- Coombs, D. S., Nakamura, Y. and Vuagnat, M. (1976) Pumpellyite-actinolite facies schists of the Taveyanne formation near Loeche, Valais, Switzerland. *Journal of Petrology*, 17, 440-471.
- Coleman, R. G. (1977) *Ophiolites: Ancient oceanic lithosphere?* Springer-Verlag, New York.
- Coleman, R. G. and Papike, J. J. (1968) Alkali amphiboles from the blueschists of Cazadera, California. *Journal of Petrology*, 9, 105-122.
- Deer, W. A., Howie, R. A. and Zussman, J. (1978) *Rock-Forming Minerals, Vol. 2A. Single-chain silicates*. London, Longman.
- Droop, G. T. R. (1982) Clinopyroxene paragenesis of albite-epidote-amphibolite facies in meta-syenites from the South-eastern Tauern Window, Austria. *Journal of Petrology*, 23, 163-185.
- Enami, M. (1981) On sodic plagioclase in some rocks of the Sanbagawa metamorphic belt in the Bessi district, Shikoku,

- Japan. Proceedings of Japan Academy, 57, Series B, 188-193.
- Ernst, W. G. (1972) CO<sub>2</sub>-poor composition of the fluid attending Franciscan and Sanbagawa low-grade metamorphism. *Geochimica et Cosmochimica Acta*, 36, 497-504.
- Essene, E. J. and Fyfe, W. S. (1967) Omphacite in California metamorphic rocks. *Contributions to Mineralogy and Petrology*, 15, 1-23.
- Hashimoto, M. (1966) On the prehnite-pumpellyite meta-graywacke facies. *Journal of Geological Society of Japan*, 72, 253-265.
- Hashimoto, M., Igi, S., Seki, Y., Banno, S. and Kojima, G. (1970) Metamorphic facies map of Japan with explanatory text. Geological Survey of Japan.
- Hey, M. H. (1954) A new review of the chlorites. *Mineralogical Magazine*, 30, 277-292.
- Higashino, T. (1975) Biotite zone of Sanbagawa metamorphic terrain in the Shiragayama area, central Shikoku, Japan. *Journal of Geological Society of Japan*, 81, 653-670.
- Hirajima, T. (1983) The analysis of the paragenesis of glaucophanitic metamorphism from a model ACF system by Schreinermakers method. *Journal of Geological Society of Japan*, 89, 679-691.
- Isozaki, Y., Maejima, W. and Maruyama, S. (1981) Occurrence of Jurassic radiolarians from the pre-Cretaceous rocks in the northern subbelt of the Chichibu belt, Wakayama and Tokushima Prefectures. *Journal of Geological Society of Japan*, 87, 555-558.
- Iwasaki, M. (1963) Metamorphic rocks of the Kotu-Bizan area, eastern Shikoku. *Journal of Faculty Sciences, University of Tokyo, Sect. II*, 15, 1-90.
- Kanmera, K. (1969) Upper Paleozoic stratigraphy of the northern Chichibu belt in eastern Shikoku. Science Report of Faculty Science, Kyushu University, Geol., 9, 237-256.
- Kurata, H. and Banno, S. (1974) Low-grade progressive metamorphism of pelitic schists of the Sazare area, Sanbagawa metamorphic terrain in central Shikoku, Japan. *Journal of Petrology*, 15, 361-382.
- Liou, J. G., Maruyama, S., and Cho, M. (1985) Phase equilibria and mineral parageneses of metabasites in low-grade metamorphism. *Mineralogical Magazine*, in press.
- Matsuda, T. (1978) Discovery of the Middle-Late Triassic conodont genus *Metapolygnathus* from calcareous schist of the Sanbagawa southern marginal belt in central Shikoku. *Journal of Geological Society of Japan*, 84, 331-333.
- Nakajima, T. (1982) Phase relations of pumpellyite-actinolite metabasites in the Sanbagawa metamorphic belt in central Shikoku, Japan. *Lithos*, 15, 267-280.
- Nakajima, T., Banno, S., and Suzuki, T. (1977) Reactions leading to the disappearance of pumpellyite in low-grade metamorphic rocks of the Sanbagawa metamorphic belt in central Shikoku, Japan. *Journal of Petrology*, 18, 263-284.
- Nitsch, K. H. (1971) Stabilitätsbeziehungen von prehnit- und pumpellyit-haltigen paragenesen. *Contributions to Mineralogy and Petrology*, 30, 240-260.
- Okay, A. I. (1980) Lawsonite zone blueschists and a sodic amphibole producing reaction in the Tavsanli region, north-west Turkey. *Contributions to Mineralogy and Petrology*, 75, 179-186.
- Otsuki, M. (1980) Petrological Study of the Basic Sanbagawa Metamorphic Rocks in Central Shikoku, Japan. Ph.D. thesis, University of Tokyo.
- Schiffman, P., Elders, W. A., Williams, A. E., McDowell, S. D. and Bird, D. K. (1984) Active metasomatism in the Cerro Prieto geothermal system, Baja California, Mexico: A telescoped low pressure/temperature metamorphic facies series. *Geology*, 12, 12-15.
- Seki, Y. (1969) Facies series in low-grade metamorphism. *Journal of Geological Society of Japan*, 75, 255-266.
- Seki, Y. (1971) Lower grade stability limit of epidote in the light of natural occurrences. *Journal of Geological Society of Japan*, 78, 405-413.
- Toriumi, M. (1975) Petrological study of the Sanbagawa metamorphic rocks, Kanto Mountains, Japan. *Bulletin of University Museum, University of Tokyo*, No. 9.
- Ueda, Y., Nozawa, T., Onuki, H. and Kawachi, Y. (1977) K-Ar ages of some Sanbagawa metamorphic rocks. *Journal of Japanese Association of Mineralogy, Petrology and Economic Geology*, 72, 361-365.
- Zen, E-An (1974) Prehnite- and pumpellyite-bearing mineral assemblages, west side of the Appalachian metamorphic belt, Pennsylvania to Newfoundland. *Journal of Petrology*, 15, 197-242.

Manuscript received, October 7, 1983;  
accepted for publication, September 21, 1984.